BIOCHEMISTRY
including biophysical chemistry & molecular biology

Article

pubs.acs.org/biochemistry

Plant Alkaloid Chelerythrine Induced Aggregation of Human Telomere Sequence—A Unique Mode of Association between a Small Molecule and a Quadruplex

Saptaparni Ghosh,[†,§] Jagannath Jana,[‡,§] Rajiv K. Kar,[‡,§] Subhrangsu Chatterjee,*[,‡] and Dipak Dasgupta*[,†]

[†]Biophysics & Structural Genomics Division, Saha Institute of Nuclear Physics, Block-AF, Sector-I, Bidhannagar, Kolkata-700064, India

[‡]Department of Biophysics, Bose Institute, P-1/12 C.I.T Scheme VII M, Kankurgachhi, Kolkata-700054, India

Supporting Information

ABSTRACT: Small molecules that interact with G-quadruplex structures formed by the human telomeric region and stabilize them have the potential to evolve as anticancer therapeutic agents. Herein we report the interaction of a putative anticancer agent from a plant source, chelerythrine, with the human telomeric DNA sequence. It has telomerase inhibitory potential as demonstrated from telomerase repeat amplification assay in cancer cell line extract. We have attributed this to the quadruplex binding potential of the molecule and characterized the molecular details of the interaction by means of optical spectroscopy such as absorbance and circular dichroism and calorimetric techniques such as isothermal titration calorimetry and differential scanning calorimetry. The results show that chelerythrine binds with micromolar dissociation constant and 2:1 binding stoichiometry to the human telomeric DNA sequence. Chelerythrine association stabilizes the G-quadruplex. Nuclear magnetic resonance spectroscopy (^{1}H and ^{31}P) shows that chelerythrine binds to both G-quartet and phosphate backbone of the quadruplex leading to quadruplex aggregation. Molecular dynamics simulation studies support the above inferences and provide further insight into the mechanism of ligand binding. The specificity toward quartet binding for chelerythrine is higher compared to that of groove binding. MM-PBSA calculation mines out the energy penalty for quartet binding to be −4.7 kcal/mol, whereas that of the groove binding is −1.7 kcal/mol. We propose that the first chelerythrine molecule binds to the quartet followed by a second molecule which binds to the groove. This second molecule might bring about aggregation of the quadruplex structure which is evident from the results of nuclear magnetic resonance.

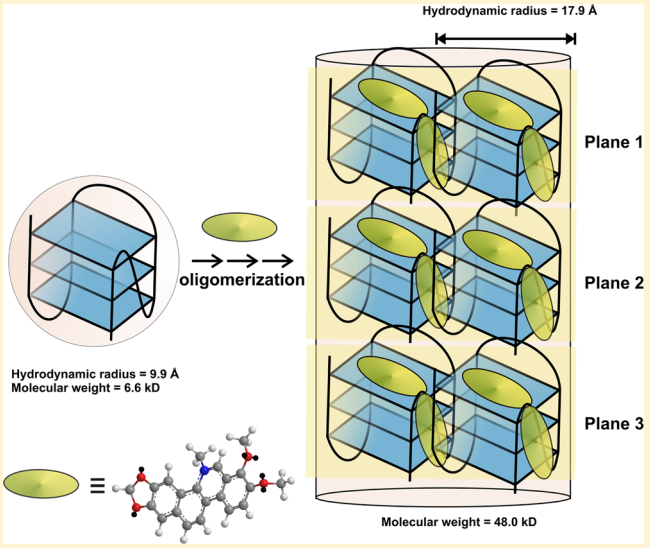

Telomeric DNA has been investigated for its role in chromosome protection, aging, cell death, and disease.[1] In humans, the telomeric tandem repeat $(TTAGGG)_n$ is found at the end of chromosomes. It can fold into a four-stranded G-quadruplex and inhibit telomerase elongation of telomeres by interrupting the interaction between the enzyme and single-stranded telomeric DNA substrate.[2,3] It thus provides a potential target for the development of new drugs in the treatment of cancer.

In solution, short fragments of the single-stranded G-rich human telomeric sequence fold to form a number of different quadruplex forms, such as chair, basket, and hybrid structures that are stabilized by a cyclic planar array of four Gs that interact via Hoogsteen hydrogen bonding called G-quartets.[4−6] The specific structure that a sequence adopts depends on the repeat length, the cation, and the length and sequence of the 5′ and 3′ tails.[4−6] For example, it has been found from nuclear magnetic resonance (NMR) studies that the oligonucleotide $d[AGGG(TTAGGG)_3]$ principally forms a basket structure in the presence of sodium ion, but converts to a mixture of hybrid-1 and hybrid-2 structures in the presence of potassium ion. It is not known with certainty which of the possible conformations of G-quartet is present as stable structures in human telomeres in vivo, or may form transiently during replication and repair. However, a few reports have shown that the hybrid form is the major form under in vivo condition.[7]

Received: September 4, 2014
Revised: December 26, 2014
Published: January 8, 2015

DOI: 10.1021/bi501117x
Biochemistry 2015, 54, 974−986

To-date, various small molecules with large planar π-aromatic surface have been tested and identified as efficient G-quadruplex binding and stabilizing agents. Herein we have reported the interaction of the human telomeric DNA sequence with the benzophenanthridine, chelerythrine (CHL, Figure 1A), a plant alkaloid with anticancer potential. The anticancer

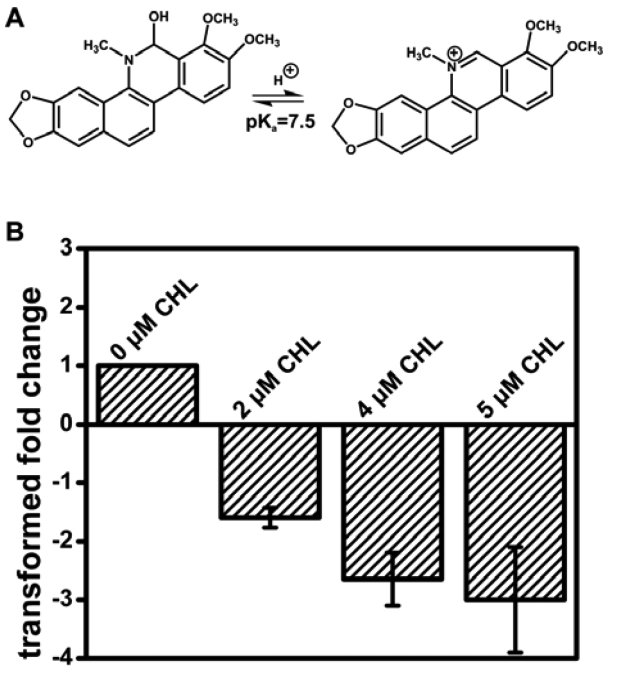

Figure 1. (A) Chemical structure of neutral and protonated forms of chelerythrine. (B) TRAP assay using RT-PCR to determine the concentration dependent change in telomerase activity (extracted from HeLa cells). Experiments were run in triplicate with indicated amount of chelerythrine.

activity of CHL is attributed to its ability to specifically act as a protein kinase C (PKC) inhibitor,[8] but contrary reports are also available.[9] In this work, we report for the first time the ability of CHL to inhibit telomerase activity. Furthermore, we have used various high resolution NMR and low resolution spectroscopic and calorimetric techniques to understand the molecular basis of interaction of CHL with human telomeric DNA sequence (H24) and elucidate the structural details of the complex formed. In addition, the experimental information as elucidated in our study has been correlated with the theoretical studies employing docking and molecular dynamics simulation to understand the binding behavior of CHL with human telomeric DNA. The G-quadruplex structure, H24, is found to bind with two CHL molecules; while the first CHL molecule binds to the G-quartet face of the quadruplex the second binds to the groove of the quadruplex. We have shown that the electrostatic interaction of these two CHL molecules is significantly different. We have also shown that the first CHL molecule stabilizes the quadruplex structure to a greater extent than the second one which binds to the loop region. The unique feature of the association is that CHL induces aggregation of H24.

EXPERIMENTAL SECTION

Materials and Preparation of Stock Solutions. CHL, potassium phosphate monobasic, potassium phosphate dibasic, potassium chloride, and desalted and HPLC purified human telomeric DNA sequence (H24, 5′-TTAGGGTTAGGG-TTAGGGTTAGGG-3′) and complementary sequence of H24 (H24comp, 5′-CCCTAACCCTAACCCTAACCCTAA-3′) were purchased from Sigma Chemical Corporation. All buffers were prepared in Milli-Q water from a Millipore Water System, Millipore, and filtered through 0.1 μm filters from Millipore prior to use. All experiments were performed in 10 mM potassium phosphate buffer (pH 6.8) containing 150 mM KCl unless otherwise mentioned.

CHL was dissolved in 10 mM pH 6.8 potassium phosphate buffer to prepare a 4 mM stock solution. The solution was stored at 4 °C and used within 2 weeks. H24 was folded into the quadruplex and duplex structures, and their concentration determined by absorbance at 260 nm as detailed in a previous study by Ghosh et al.[10]

Telomerase Repeat Amplification Protocol (TRAP Assay). Cell extracts from HeLa cell lines were used to perform the SYBR Green RQ-TRAP assay with SYBR Green PCR Master Mix (US Biomax, INC-Telomerase Detection Kit-MT3012) as reported previously.[10,11] The transformed fold change in telomerase activity with varying CHL concentration was determined from the threshold cycle values.[10,11]

Absorption Spectroscopy. Absorption spectra were measured in a CECIL spectrophotometer. CHL (10 μM) was titrated with increasing amounts of H24 until saturation was reached (an equal amount of DNA was added to the reference cell during titration) to determine dissociation constant of the interaction. Readings were noted 5 min after each addition to ensure complete complex formation. The binding isotherm was generated by plotting $\Delta A/\Delta A_{max}$ at 316 nm as a function of H24 concentration. The experimental points obtained were fitted using the equation[12]

$$C_0(\Delta A/\Delta A_{max})^2 - (C_0 + C_p + K_d)(\Delta A/\Delta A_{max}) + C_p = 0 \quad (1)$$

where C_0 is the initial concentration of CHL, ΔA is the change in absorbance at 316 nm for each addition of H24, ΔA_{max} is the same parameter when CHL is totally bound to H24, and C_p is the concentration of H24 added. The X-intercept value at $\Delta A/\Delta A_{max}$ = 0.5 (corresponding to 50% binding) gives the dissociation constant, K_d. ΔA_{max} was determined from the double reciprocal plot of $1/\Delta A$ against $1/(C_P - C_0)$ using the equation[12]

$$1/\Delta A = 1/\Delta A_{max} + 1/(C_p - C_0) \quad (2)$$

Method of continuous variation (Job Plot)[13] was also employed to determine the stoichiometry of CHL−H24 complex by monitoring absorbance of CHL at 316 nm for reaction mixtures, in which the number of moles of H24 and CHL in a fixed volume was varied, keeping the sum total number of moles constant.

Isothermal Titration Calorimetry. ITC experiments were done in a iTC200 Microcalorimeter, Microcal Inc., at different temperatures between 10 and 35 °C. Samples were extensively degassed prior to titration. H24 was injected into a fixed concentration of CHL (25 μM). A blank experiment in which H24 was injected into buffer with no CHL was carried out to correct the data due to dilution. Background was subtracted from the measured heats, and the corrected heats were plotted against molar ratio. The corrected isotherms showed that only one type of binding event is taking place. The isotherms were analyzed using the in-built Microcal LLC ITC software. "One set of sites" model yield the best fitted curve for the obtained

DOI: 10.1021/bi501117x
Biochemistry 2015, 54, 974−986

data points. Equilibrium association constant (K_a), enthalpy (ΔH), and entropy (ΔS) of association were obtained after fitting the isotherms. The Gibbs Energy was calculated using the equation

$$\Delta G = \Delta H - T\Delta S \quad (3)$$

Change in heat capacity (ΔC_p) for the association of CHL with H24 was calculated from the slope of the plot of enthalpy change (ΔH) against temperature. To determine the extent of enthalpy−entropy compensation, the slope of ΔH versus $T\Delta S$ was determined.

To determine the binding parameters for H24 duplex DNA to CHL, 25 μM CHL was titrated with increasing duplex until saturation was reached at 25 °C. To maintain the ionic strength of the solution, 150 mM KCl was added to the buffer prior to titration. The thermogram obtained was analyzed using the "one set of sites" model to determine the association constant for the interaction.

Differential Scanning Calorimetry. The heat capacity was measured as a function of temperature in a VP DSC Microcalorimeter (Microcal, LLC, Northampton, MA) to investigate the helix to coil transition of H24 and H24−CHL complex. The samples were scanned at a scan speed of 60 °C/h at approximately 30 psi pressure. Prior to sample scan, the instrument was thermally stabilized by repeated buffer scans under similar conditions. H24 at 100 μM was scanned to obtain the melting profile of the unbound form. A concentration of 70 μM H24 was incubated with 190 μM CHL for 1 h to ensure complete complex formation and scanned to obtain the melting profile of the bound form. To explore the potential of CHL to induce stability in a double stranded DNA, H24 duplex and H24 duplex−CHL complex were scanned under similar experimental conditions. The thermograms obtained were analyzed using the in-built VPViewer software with Origin 7.0. The non-2-state (cursor initiation) model of curve fitting was used to fit the raw thermograms.

Circular Dichroism. CD spectra were recorded on JASCO J715 spectropolarimeter (Jasco Cooperation, Tokyo, Japan) at 25 °C. The CD scans were recorded within the wavelength range of 220−420 nm with scan speed 200 nm/min and step size of 0.1 nm. The time constant was 2 s, and bandwidth was 1 nm. All measurements were carried out in a 0.1 cm path length cuvette in a reaction volume of 300 μL. A concentration of 20 μM H24 was titrated with increasing concentration of CHL. Each reading was an average of four runs. Readings were noted 5 min after each addition to ensure complete complex formation. Convex constraint analysis (CCA) was performed on the spectral set in order to extract the basis spectra and their associated coefficients.[14]

NMR Spectroscopy. All NMR spectra were recorded using Bruker AVANCE III 500 MHz NMR spectrometer equipped with a 5 mm SMART probe at 298 K. Data processing and acquisition were performed with Topspinv3.1 software. NMR samples were prepared in 10 mM potassium phosphate buffer, 150 mM KCl at pH 6.8 containing 10% D_2O. DSS (2, 2-dimethyl-2-silapentane 5-sulfonate sodium salt) was used as an internal standard (0.0 ppm).

A series of one-dimensional proton spectra of H24 were recorded with increasing concentration of CHL up to 1:2 (H24/CHL) ratio using Bruker Pulprog "zgesgp" with a spectral width of 20 ppm, number of scans of 512, and calibrated pulse length of 12.79 us. One-dimensional temperature induced melting of imino proton experiments were performed using the same acquisition parameters at an interval of 10 °C from 25 to 75 °C. To know the interaction between phosphate backbones of H24 and CHL, one-dimensional proton-decoupled ^{31}P NMR spectra of H24 were performed with increasing concentration of CHL up to 1:2 (H24/CHL) ratio using Bruker pulse program "zgpg30". Total number of scans for ^{31}P NMR was 512. The hydrodynamic radius and molecular weight of free H24 and H24−CHL complex were determined by diffusion order NMR spectroscopy (DOSY).[15,16] Sodium acetate (1 mM) was added into the solution of free H24 and H24−CHL complex as an internal reference. A total of 24 one-dimensional ^{1}H NMR spectra were recorded with increasing gradient strength from 5% to 95% for both cases (free and complex DNA) using Bruker Pulse program "stebpgp1s191d" (a diffusion measurement using stimulated echo) with a spectral width of 20 ppm and 128 scans with 4 dummy scans. The decay of the intensity of ^{1}H signals from H24 were plotted using equation

$$I(g) = Ae^{dg^2} \quad (4)$$

where I, g, and d represent intensity of the peak, gradient strength, and decay rates, respectively. The hydrodynamic radius were measured using the equation

$$R_h = d_{ref}/dR_h^{ref} \quad (5)$$

where R_h is the hydrodynamic radius of DNA (free or complexed), d_{ref} is the decay rate of reference, and d is the decay rate of DNA (free or complexed). R_h^{ref} was taken to be 2.3 Å. The molecular weight of free and complexed DNA were determined using the equation

$$\log(d1/d2) = (1/3)\log(MW2/MW1) \quad (6)$$

All the spectra were processed and zeroth and first order phase correction manually.

Structure Generation and Docking Calculation. H24 is reported to adopt a (3 + 1) hybrid-1 structure.[17] Based on this assumption, the NMR resolved solution structure of a 23-mer G-rich DNA, sequence [TAGGG(TTAGGG)$_3$], was adopted to copy the set of coordinates (pdb code 2jsm) for structure generation. H24 structure was built using Maestro by addition of a thymine residue at the 5′ end taking care of the glycosides torsion angels. The process was accompanied by gas-phase energy minimization for removal of any steric clashes and rectification in bond orders.

Docking calculation of CHL with H24 was carried out in Glide module using Standard Precision (SP) mode (Glide, version 5.5, Schrödinger, Inc., New York, NY, 2009).The grid was prepared by covering the entire structure of prepared H24 with dimensions of 80 × 80 × 80 Å^3. The first round of docking was used to obtain a 1:1 complex where the molecule prefers to bind at the quartet face. This 1:1 complex of CHL and H24 was used as a receptor in the second round to obtain the 1:2 complex. The second ligand binds to the groove region. Adaptive Poisson−Boltzmann Solver (APBS) equation was used to illustrate the electrostatic potential basis of the molecular interaction between CHL and H24.[18] These results help to correlate the dielectric properties with the spatial distribution of partial atomic charges in the macromolecular complex. Electrostatic distribution was visualized with counters for electropositive and electronegative iso-surface at +10 and −10 kT/e values.

DOI: 10.1021/bi501117x
Biochemistry 2015, 54, 974−986

Molecular Dynamics Simulations. MD simulations were carried out in Amber11 using the parmbsc0 modifications in conjunction to the ff99 force field for H24.[19,20] Simple harmonic function used by the General Amber Force Field (GAFF) with AM1-BCC charge model was used for the parametrization of CHL.[21] K^+ ions were accommodated in the central core of H24. They were also used for counter-stabilizing the charge of the solvated system. Parameters of K^+ ions were adopted from Dang's work.[22] The system was further solvated in a octahedral box using TIP3P water model with edge length extension of 10 Å from solute atom.[23] Simulations were carried out using periodic boundary conditions with particle mesh Ewald summation method[24] to compute the electrostatic contributions with grid spacing of approximately 1 Å. The long-range van der Waals interactions were corrected using a cutoff value of 9 Å for Lennard–Jones potential and direct space interactions. SHAKE algorithm with tolerance threshold of 10^{-5} Å was used for restraining hydrogen atoms with integration time step of 2 fs.[25] In total, three simulations were carried out: (i) H24 as control system; (ii) CHL and H24 in 1:1 complex; and (iii) CHL and H24 in 1:2 complex.

The simulation protocol was adopted from the work of Islam et al.[26] The energy minimization was performed in explicit solvent conditions with steepest descent followed by conjugate gradient steps. H24 and corresponding CHL–H24 complexes were restrained for a time scale of 300 ps, and the solvent molecules were equilibrated. The temperature of the system was increased gradually from 0 to 300 K with time interval of 0.5 ps. Finally the constraints were gradually decreased until there were no further applied restrains. This helps the system to attain complete equilibrium. The production run was continued up to a time scale of 100 ns for all systems, with trajectory collection at an interval of 2 ps. The analysis of the MD trajectory was performed using cpptraj module of Amber-tools14.[27]

Binding Energy Calculation. MM-PBSA method was used to calculate the free energy and binding energies.[28,29] Details of the methodology have been given in the Supporting Information.

RESULTS

Telomerase Repeat Amplification Protocol. TRAP assay was done using quantitative real time PCR to study the in vitro effect of CHL on telomerase activity by targeting quadruplex DNA. As shown in Figure 1B, CHL causes a dose dependent decrease in telomerase catalytic activity in cell lysate prepared from HeLa cell line. During real time TRAP, the number of threshold cycles required to obtain a detectable level of fluorescence intensity increased. This was used to quantify the dose dependent decrease in telomerase activity. Telomerase activity decreases by 1.5-fold on addition of 2 μM CHL and by 3-fold on addition of 5 μM CHL to the cell extracts. Our results show that CHL negatively affects the typical six nucleotide ladder (TTAGGG) of primer extension products characteristic of human telomerase in TRAP assay.

Absorption Spectroscopy. The absorbance of CHL at 316 nm decreases on binding to H24 and is accompanied by a red shift of the peak by about 12 nm (Figure 2A, inset), as a result of its association with the quadruplex. The dissociation constant was determined to be 2.3 ± 0.3 μM from absorbance of CHL at 316 nm (Figure 2A).

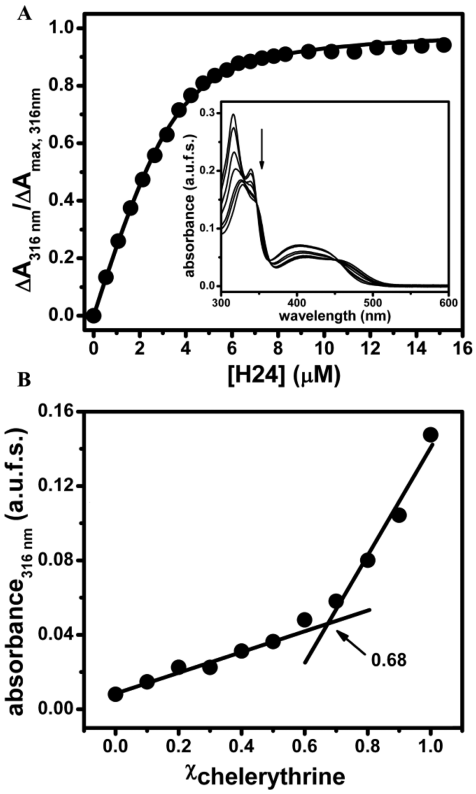

Figure 2. (A) Curve fitting analysis of the binding isotherm obtained from absorption titration to evaluate the dissociation constant for the association of chelerythrine with H24. Inset: Absorption spectra of chelerythrine in the presence of increasing concentration of H24. (B) Job plot to determine the binding stoichiometry for association of chelerythrine with H24. All experiments were done at 25 °C in 10 mM potassium phosphate buffer (pH 6.8) containing 150 mM KCl.

The method of continuous variation also shows a 2:1 (H24/CHL) binding stoichiometry for H24–CHL complex (Figure 2B).

Isothermal Titration Calorimetry. The thermodynamic parameters for the association of H24 with CHL at different temperatures are presented in Table 1. The representative thermogram for the interaction is shown in Figure 3A(i). Both enthalpy and entropy contribute favorably towards the association. The reaction enthalpy and entropy decreases linearly with temperature (Figure 3A(ii), Table 1). A slope of nearly unity for the ΔH versus $T\Delta S$ plot indicates that the association proceeds with enthalpy–entropy compensation (Figure 3A(iii), Table 1). Moderately high negative ΔC_p value characterizes the association of CHL with H24 and was determined from the slope of ΔH versus temperature (Figure 3A(ii), Table 1).

The thermodynamic parameters obtained for interaction of H24 duplex with CHL (Figure S1, Supporting Information) are listed in Table 1.

Differential Scanning Calorimetry. To examine the thermal stability of H24 in the absence and presence of CHL, DSC was done. The results show that ligand binding stabilizes H24. The melting parameters obtained for H24 in the free and ligand bound state are summarized in Table 2. Free H24 shows two melting transitions as reported earlier (Figure 3B(i)).[30] In contrast, the ligand bound form has a single melting transition at higher temperature (Figure 3B(ii)).

DOI: 10.1021/bi501117x
Biochemistry 2015, 54, 974–986

Table 1. Variation of Thermodynamic Parameters for the Association of H24 with Chelerythrine at Different Temperatures As Determined by ITC

T (°C)	K_a ($\times 10^5$ M^{-1})	ΔH (kcal/mol)	$T\Delta S$ (kcal/mol)	ΔG (kcal/mol)	ΔC_p (cal/mol/K)	EEC slope
10	4.3 ± 1.2	−3.3 ± 0.1	4.0	−7.3	−117.5 ± 7.0	1.1 ± 0.0
15	5.2 ± 1.4	−3.8 ± 0.1	3.8	−7.6		
20	3.8 ± 0.6	−4.7 ± 0.1	2.8	−7.5		
25	3.9 ± 0.3	−5.0 ± 0.1	2.6	−7.6		
	0.3 ± 0.1[a]	−4.0 ± 0.3[a]	2.2[a]	−6.2[a]		
30	3.9 ± 0.2	−5.7 ± 0.1	2.0	−7.7		
35	2.7 ± 0.3	−6.2 ± 0.1	1.5	−7.7		

[a]Thermodynamic parameters for the interaction of chelerythrine with H24 duplex.

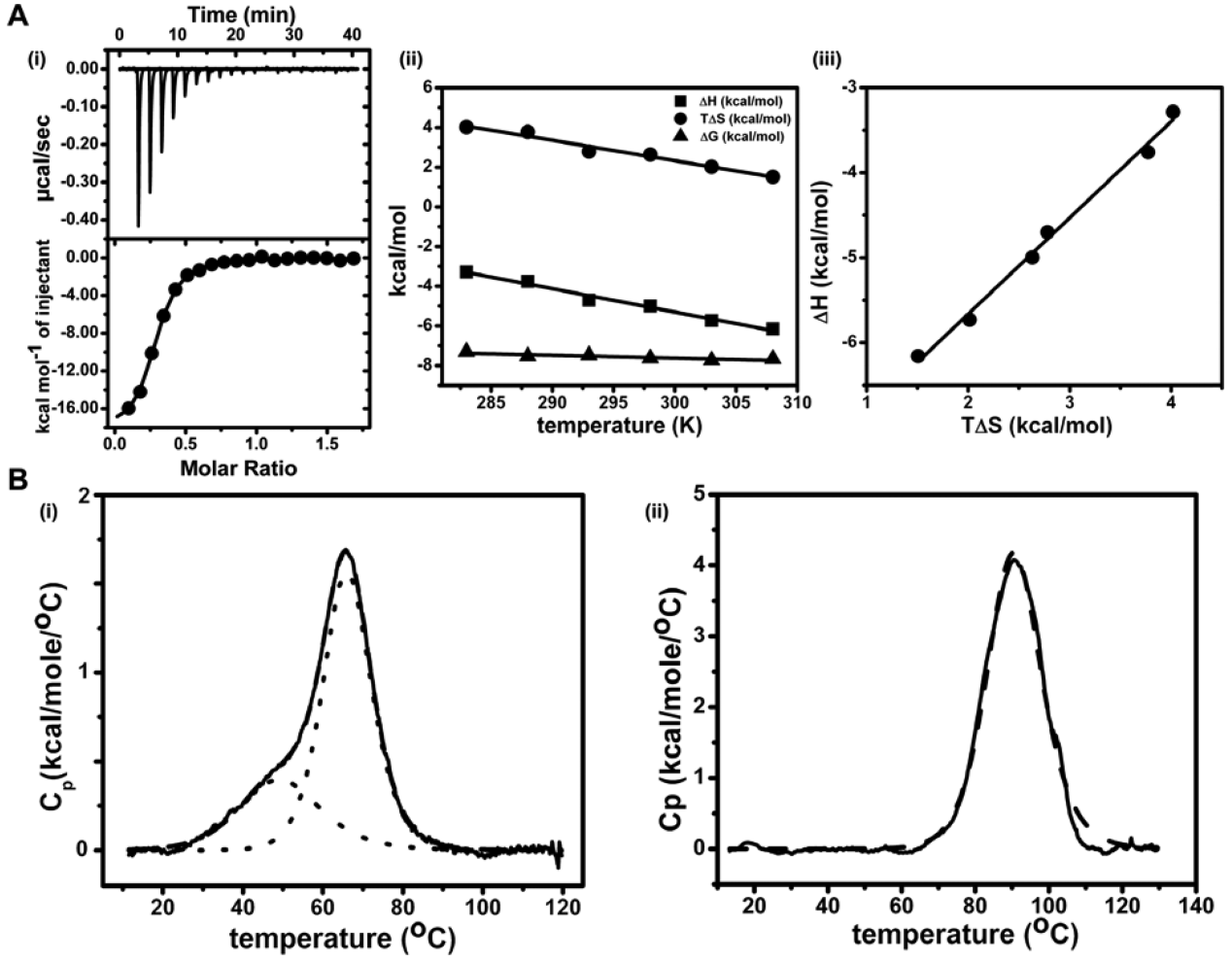

Figure 3. (A) (i) Representative ITC profile for the titration of 25 μM chelerythrine with H24 at 25 °C. The upper panel shows the change in differential power (DP) of the instrument. Bottom panel shows the binding isotherm resulting from integration of the peak area as a function of molar ratio. The solid line represents the calculated fit of the data. (ii) Variation of thermodynamic parameters with temperature for the association of chelerythrine with H24. Linear temperature dependence of enthalpy yields ΔC_p. (iii) Enthalpy−entropy compensation plot for the interaction of chelerythrine with H24. (B) Excess heat capacity profile for (i) 100 μM H24 in the absence of chelerythrine and (ii) 70 μM H24 in the presence of saturating chelerythrine concentration (190 μM). The observed data (solid line) were deconvoluted (dotted lines) using the inbuilt "2-state" model for curve fitting software. The dashed curve denotes the overall fit of the data. ITC and DSC experiments were carried out in in 10 mM potassium phosphate buffer (pH 6.8) containing 150 mM KCl.

CHL does not impart any stability to H24 duplex upon binding as evident from similar melting temperatures for the free and CHL bound forms (Figure S2, Supporting Information).

Circular Dichroism. H24 folds into a (3 + 1) hybrid structure in the presence of potassium ions characterized by the following CD features: a major positive band at 290 nm, a hump at 268 nm, and a minor negative band at 236 nm (Figure 4A, spectrum in black). Intensity of the two signature peaks at 290 and 236 nm increases while that at 268 nm decreases upon complex formation with CHL (Figure 4B).

CCA analysis of the set of CD spectra obtained for H24 CHL interaction could be best deconvoluted into two basis spectra (Figure 4C). The first and second components are

DOI: 10.1021/bi501117x
Biochemistry 2015, 54, 974−986

Table 2. Thermodynamic Parameters for Intramolecular Quadruplex to Random Coil Transition, in the Absence and Presence of Saturating Concentration of Chelerythrine, for H24 in 10 mM Potassium Phosphate Buffer (pH 6.8) Containing 150 mM KCl As Determined by DSC

system	T_{m1} (°C)	ΔH_{cal1} (kcal mol^{-1})	T_{m2} (°C)	ΔH_{cal2} (kcal mol^{-1})
H24	49.5 ± 0.2	10.7 ± 0.2	66.2 ± 0.0	25.3 ± 0.2
H24−CHL	90.7 ± 0.0	82.1 ± 0.3		

characteristic of the CD spectra of free H24 and CHL bound form of H24, respectively. The variation of the associated coefficients of each basis spectrum shows a decrease in the percent population of component 1 with a concomitant increase in the percent population of component 2 as a function of CHL concentration (Figure 4D).

NMR Spectroscopy. The electronic environment of the individual guaninyl residues is assumed to be nonequivalent. A record of the melting of *N1−H* imino protons of H24 as a function of temperature shows that G-16 and G-24 melt relatively faster than others (Figure S3, Supporting Information). This observation implies that these Gs are exposed to surrounding water.

The high resolution NMR experiments were performed to characterize the interaction between H24 and CHL and throw light on the structure of the complex. One-dimensional imino proton spectra of free H24 is a signature of hybrid type quadruplex structure under physiologically relevant condition.[17] Figure 5 shows an array of one-dimensional imino proton spectrum of H24 with increasing concentrations of CHL up to 1:2 (H24/CHL) ratio. In the absence of CHL, H24 exists in a monomeric, globular, and folded conformation as indicated from sharp imino signals of 12-guaninyl residues. Progressive addition of CHL to this folded conformation led to disappearance of most of the imino signals of guaninyl residues up to a ratio of 1:1. Interestingly, some of the imino peaks started to appear with relatively broader line width when the concentration of CHL was further increased. When CHL was added to H24 at 2:1 ratio, we noticed new imino peaks arising at different resonance positions. These peaks have relatively greater intensity compared to the imino protons corresponding to a lower input ratio.

One-dimensional proton decoupled ^{31}P NMR experiments were carried out to show the interaction between the phosphate backbone of H24 and CHL. Figure S3 (Supporting Information) shows an array of one-dimensional ^{31}P NMR spectrum of H24 and its complex with increasing concentrations of CHL up to a molar ratio of 2:1 (CHL/H24). One-dimensional ^{31}P NMR spectra (Figure S4, Supporting Information) of H24 showed a ^{31}P intensity drop, substantial broadening, perturbation in the chemical shifts upon addition of CHL.

The hydrodynamic radii of free and CHL bound H24 were estimated to be 9.9 and 17.9 Å, respectively, by means of DOSY. The calculated molecular weights of free and CHL bound H24 were found to be 6.6 and 48.0 kDa, respectively.

Molecular Dynamics Simulation. The first round of docking procures the 1:1 binding complex. In this complex,

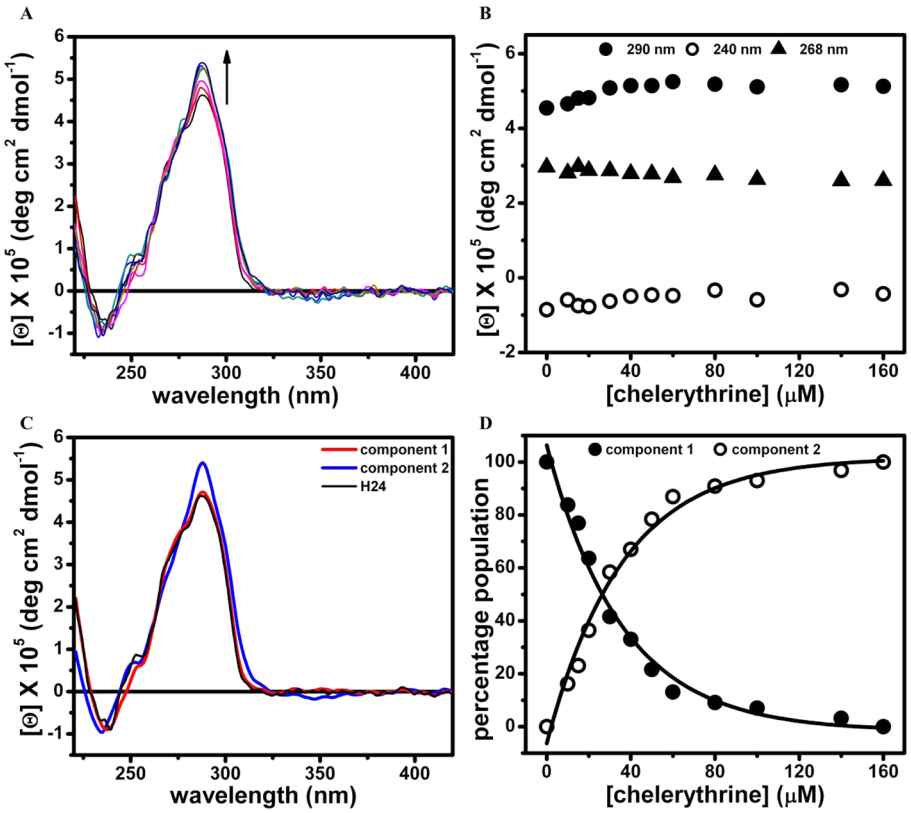

Figure 4. (A) Representative CD spectra resulting from the interaction of H24 (20 μM, spectrum in black) with increasing chelerythrine concentration in 10 mM potassium phosphate buffer (pH 6.8) containing 150 mM KCl at 25 °C. (B) Variation in the molar ellipticity value at three selected wavelengths, 240, 268, and 290 nm, for the interaction. (C) Basis spectra obtained from CCA analysis of CD spectra shown in (A). (D) Contribution of CCA components as a function of chelerythrine concentration.

DOI: 10.1021/bi501117x
Biochemistry 2015, 54, 974−986

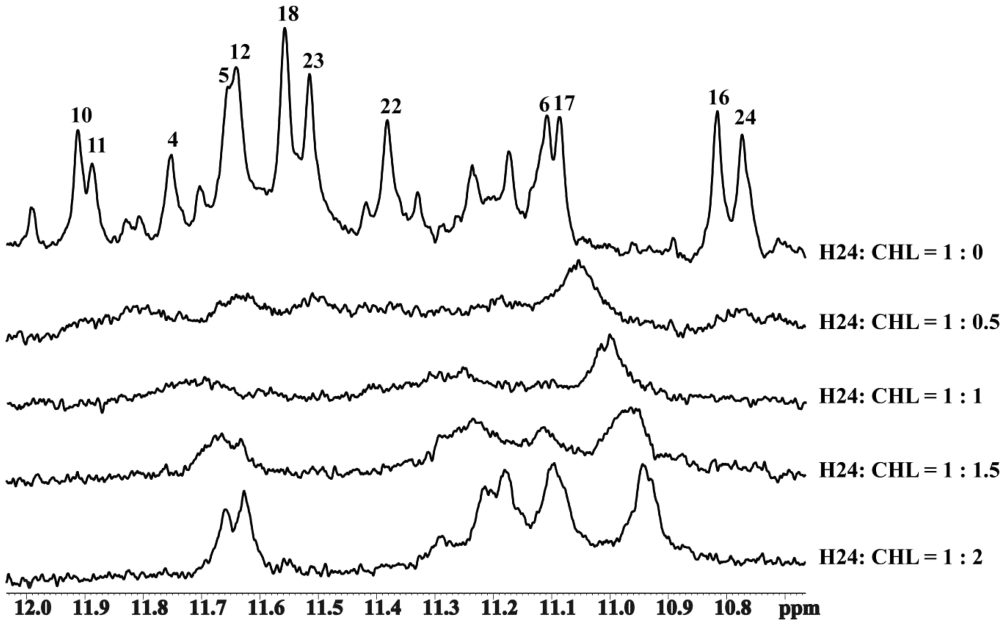

Figure 5. One-dimensional imino proton resonance spectra of H24 with increasing concentration of chelerythrine (CHL).

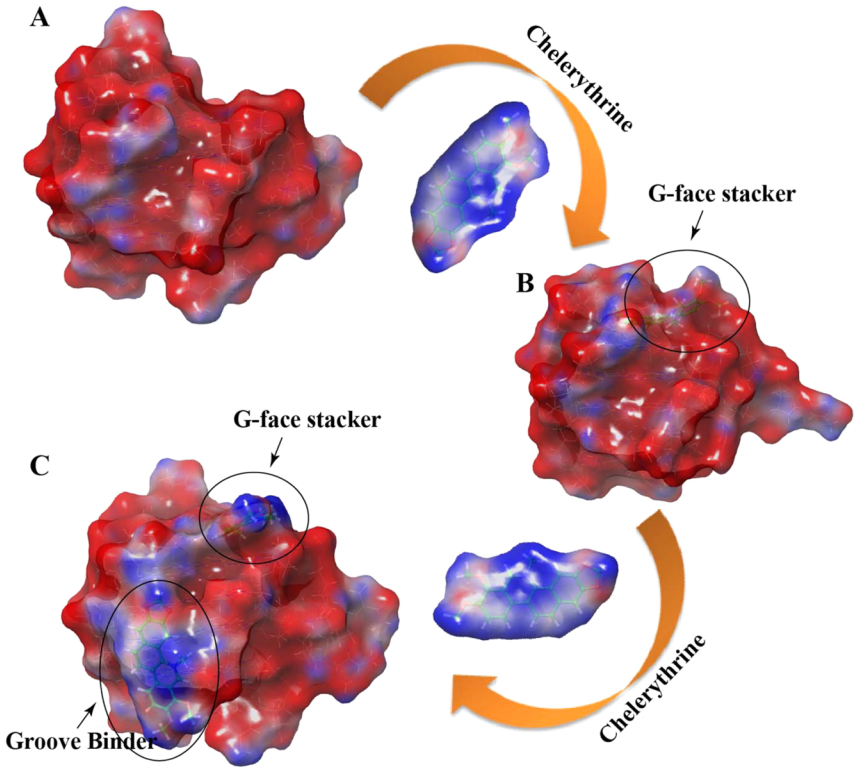

Figure 6. Electrostatic model of (A) control H24, (B) H24–chelerythrine (1:1) complex, and (C) H24–chelerythrine (1:2) complex computed by solving the Adaptive Poisson–Boltzmann Solver. The complex system was shown with a transparent surface model having red and blue contours representing electronegative and positive isosurfaces, respectively, at ±10 kT/e.

CHL binds to the quartet plane with the two methoxy groups protruding towards the quartet plane and the benzodioxolo group towards the solvent. Figure 6B gives an overview where CHL stacks on the quartet plane. Bases G6 and G24 are involved in the stacking interaction. In the second round of docking studies, this complex was used as a receptor and docked with CHL. It was found that the second CHL molecule binds in the groove region (Figure 6C). It is interesting to note that in both cases no sustainable hydrogen bonding was found between CHL and H24. The association of CHL with H24 is stabilized by the face-to-face and face-to-edge stacking in quartet and groove binding postures, respectively.

APBS was used to elucidate the electrostatic contributions in the binding of CHL with H24. Electrostatic contours suggest CHL to be highly electropositive and H24 to be mostly electronegative. Analysis of the 1:1 complex indicates that the

DOI: 10.1021/bi501117x
Biochemistry 2015, 54, 974–986

electrostatic interaction stabilizes these counter potentials. Negative charge of H24 diffuses out when CHL stacks over the G-quartet face (Figure 6A and B). This diffusion of charges seems to be more pronounced when the second CHL molecule binds to the groove region (Figure 6C). Notably, the inference of the charge and the interaction phenomenon obtained is based on static model but the actual property of biomolecule depends on the dynamicity. The physicochemical properties of macromolecule in a solvent cage are used to predict crucial and reliable information on conformational hyperspace and solvent solute integrity. We have used molecular dynamics simulation technique in explicit solvent condition to obtain a clear picture for the isolated behavior of H24 in complex with CHL molecules.

In the course of MD simulation, CHL was found to adjust its position compared to its initial docked state being interacted with the explicit solvent as the medium. After the initial equilibration step with small force constant restraints over H24 atoms, the methoxy groups of CHL were found to protrude towards the solvent. Within the initial 2−3 ns, the position of the bezodioxolo group was adjusted and it came in close proximity to the quartet. To understand the stability of the complex, a root mean squared deviation (rmsd) plot has been generated for all the three systems: (1) control H24, (2) 1:1 (H24/CHL), and (3) 1:2 (H24/CHL) (Figure S5, Supporting Information). Compared to free H24, the rmsd plots for the atoms in 1:1 and 1:2 complexes seem to be more stabilized. The initial jump in the rmsd data point with respect to the starting frame of reference can be attributed to the adjustment of the solute with respect to explicit solvent condition. There is also a variation in the rmsd plot for heavy atoms of H24 in the 1:2 complex, which can be attributed to the loose binding of groove bound ligand.

Results from low resolution spectroscopic studies presented above show that CHL binds to the quadruplex structures with 2:1 binding stoichiometry. These experimental results and the MD simulation data can be combined to propose that CHL binds to H24 in two plausible ways: (i) First, one CHL molecule binds to the surficial G-quartet face of the quadruplex, and then the second CHL binds to the groove. (ii) Alternately, first a CHL molecule binds to the groove of quadruplex, followed by the second CHL molecule binding to the surficial G-quartet face of the quadruplex. The binding energies of CHL with quadruplex for 1:1 and 2:1 complexes (formed by both the above-mentioned mechanisms) were determined using AMBER based MMPBSA calculation and are tabulated in Table 3.

Table 3. Thermodynamic Parameters,[a] Calculated Using MMPBSA Method from 300 ns Simulation Data

	1:1 complex	1:2 complex[b]	1:2 complex[c]
ΔE_{elec}	−542.1 ± 11.5	−490.4 ± 29.1	−459.4 ± 78.7
ΔE_{vdw}	−40.1 ± 3.0	−27.0 ± 10.0	−21.6 ± 8.3
ΔE_{mm} (ΔE_{elec} + ΔE_{vdw})	−582.2 ± 9.2	−517.3 ± 20.6	−481.1 ± 60.1
ΔG_{PB}	581.6 ± 13.2	512.7 ± 33.5	478.7 ± 40.3
ΔG_{np}	−29.7 ± 1.2	−15.3 ± 1.9	−12.4 ± 1.6
ΔG_{solv} (ΔG_{np} + ΔG_{PB})	551.9 ± 11.9	497.4 ± 15.3	466.4 ± 23.6
ΔG_{total} (ΔE_{mm} + ΔG_{solv})	−30.3 ± 3.1	−19.9 ± 1.0	−14.6 ± 1.2
$-T\Delta S$	−16.7 ± 2.0	−15.2 ± 3.5	−12.9 ± 2.8
ΔG_{bind} ($\Delta G_{total} - T\Delta S$)	−13.6 ± 1.2	−4.7 ± 1.0	−1.7 ± 0.8

[a]Energy values are given in kcal/mol. [b]Calculations are made using quartet binding chelerythrine as ligand, and groove binding chelerythrine is considered as part of receptor. [c]Calculations are made using groove binding chelerythrine as ligand, and quartet binding chelerythrine is considered as part of receptor.

DISCUSSION

Reports available so far suggest that the anticancer activity of the plant alkaloid CHL is linked to its ability to inhibit protein kinase C.[8] In this report, we have investigated the potential of CHL to bind to the quadruplex structure formed by the human telomeric sequence, which can be an additional mechanism by which the molecule exerts its anticancer property. The current study focuses upon the molecular basis of its association with the human telomere repeat H24-5′-TTAGGGTTAGGG-TTAGGGTTAGGG-3′. It may be mentioned that there is an earlier report of the association of CHL with a nontelomeric quadruplex with a difference sequence, d(AGGGAGGGCGCT-GGGAGGAGGG).[31] This report showed the binding using ESI-MS and CD followed by an in silico autodock3. However, this report does not indicate any ligand-induced aggregation of the G-quadruplex, nor does it demonstrate telomerase inhibitory potential by TRAP assay. Both of our findings are, therefore, more relevant to understand the potential of CHL as a telomerase inhibitor.

Telomerase from HeLa cell line extract adds the human telomeric repeat unit at the end of the TS primer which is capable of adopting a quadruplex structure. Figure 1B shows that CHL blocks telomerase activity in a concentration dependent manner. This indicates that CHL interacts with the quadruplex structure formed at the end of TS primer. We have used spectroscopic and calorimetric techniques to study the molecular basis of this interaction and characterize the complex formed as a result of the association of CHL with human telomeric DNA. These studies have been supplemented with molecular dynamics simulation to understand the complex formation phenomenon.

The observed red shift in the CHL spectrum upon H24 binding can be attributed to the stabilization of the π^* orbital of CHL leading to a reduced energy gap for $\pi \rightarrow \pi^*$ transition. Such stabilization has been reported earlier for other small quadruplex binding molecules and can be due to either end stacking on the quartets or intercalative mode of binding.[10] The observed binding stoichiometry of 2:1 indicates that two CHL molecules bind to the quadruplex.

From the thermodynamic perspective, the favorable free energy change of association of H24 with CHL results from negative enthalpic and positive entropic contributions. A slope of near unity for the ΔH versus $T\Delta S$ plot indicates that the association of H24 with CHL proceeds with enthalpy−entropy compensation. Noncovalent interactions like stacking is associated with negative enthalpy contributions. The entropy change associated with the interaction can be ascribed to two mutually opposing trends: (a) increase in entropy due to release of water molecules and/or conformational changes in H24 structure upon CHL binding and (b) decrease in entropy from the configurational change in H24 due to complex formation as shown by NMR. The increase in entropy from release of water molecules can override the decrease in configurational entropy arising from ordering of the bound telomere molecules. It leads to net positive entropy that contributes favorably toward the free energy change of the

DOI: 10.1021/bi501117x
Biochemistry 2015, 54, 974−986

Scheme 1. Schematic Representation of a Single Unit Involved in Oligomerization of H24 in the Presence of Chelerythrine

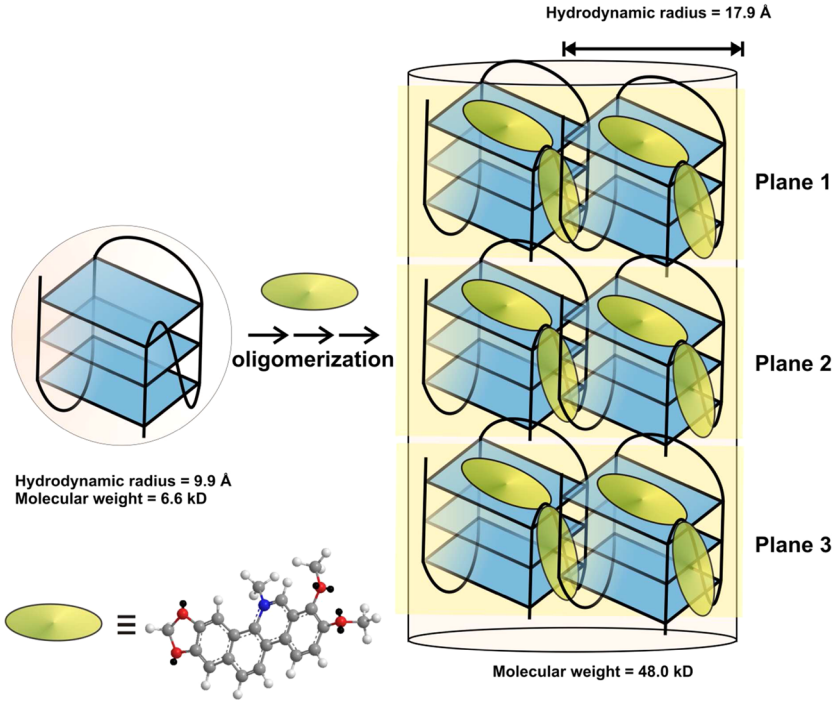

association. Variation of enthalpy with temperature yield moderately high negative ΔC_p for binding of CHL to H24. This could be attributed to (a) burial of water accessible hydrophobic surface area, which gives rise to the release of bound water and/or the release of counterions[32,33] and (b) destacking of bases in the loop regions of the quadruplexes as a sequel to the stacking interaction between the planar CHL moiety and bases of the G-quartets.[34] High ΔC_p values indicate a greater contribution of ΔG_{hyd} as evident from the following relation[35]

$$\Delta G_{hyd} = (80 \pm 10)\Delta C_p$$

Though we report that CHL has two potential binding sites for binding to H24, the ITC thermograms could not be analyzed using the "two sets of sites" model. This can be accounted by the fact that the binding affinity of CHL for these two sites is comparable. This is also corroborated from the MMPBSA calculations which show that the binding energy of the 1:1 and 1:2 complexes are similar. Under these conditions, the reported affinity values reflect an average of the binding affinities for both the sites. Our results furthermore show that CHL has a higher affinity for the quadruplex structure than the duplex structure. Also, CHL binding does not impart any stability to duplex structure. We however refrain to quantify the specificity of CHL toward H24 based on these data.

The enhanced melting temperature of H24 upon ligand association indicates that CHL binding stabilizes H24. While H24 shows two melting transitions H24−CHL complex has only one melting transition. The two melting transitions for free H24 are due to the three-state melting process of H24. In this, there is a gradual disappearance of one species with the concurrent appearance of the second species and concerted formation and disappearance of the transient species. Melting studies of H24−CHL complex was carried out at a ratio of the two components to ensure complete formation of the complex between them. As evident from the NMR studies at this ratio, CHL causes aggregation of H24. The aggregated species melts as a single unit. The single melting transition obtained for H24 in the bound form results from one type of complex that forms between H24 and CHL. Thus, the CD signature does not show any significant structural transition but we observe a single melting temperature for CHL bound H24. This is also consistent with the CCA analysis results obtained from CD data as described later.

To identify the binding mode of CHL to H24 we took help of CD and NMR spectroscopy. CD signature of H24 in K^+ is characteristic of the (3 + 1) hybrid structure. The intensity of the CD peaks increases upon interaction of H24 with CHL. To understand the structural perturbation, if any, associated with ligand binding, the CD spectral set was subject to CCA analysis. CCA analysis is an algorithm to deconvolute a set of experimentally obtained CD spectra into a set of basis spectra, combination of which can express all the experimentally obtained spectra. The minimum number of basis spectra required to fit the observed set of spectra is two. Therefore, we have resolved the observed spectra as a sum of 2 basis spectrum. The experimentally obtained spectra in this case could be best deconvoluted into two basis spectra. Component 1 has spectral features representing free H24, and component 2 represents the ligand bound form of H24. A comparison of the spectral features of components 1 and 2 shows that both have a major positive peak at 290 nm and a minor negative peak at 236 nm. However, the intensity of the hump at 268 nm is reduced in component 2 as compared to component 1. These features support the proposition of absence of any gross structural alteration of individual H24 moiety as a sequel to ligand binding. The fact that the CD spectra for H24−CHL interaction could be deconvoluted into only 2 basis spectra indicates that only a single type of complex is formed as a result of the association. The similarity of the 2 basis spectra indicates that CHL association induces insignificant structural change in

DOI: 10.1021/bi501117x
Biochemistry 2015, 54, 974−986

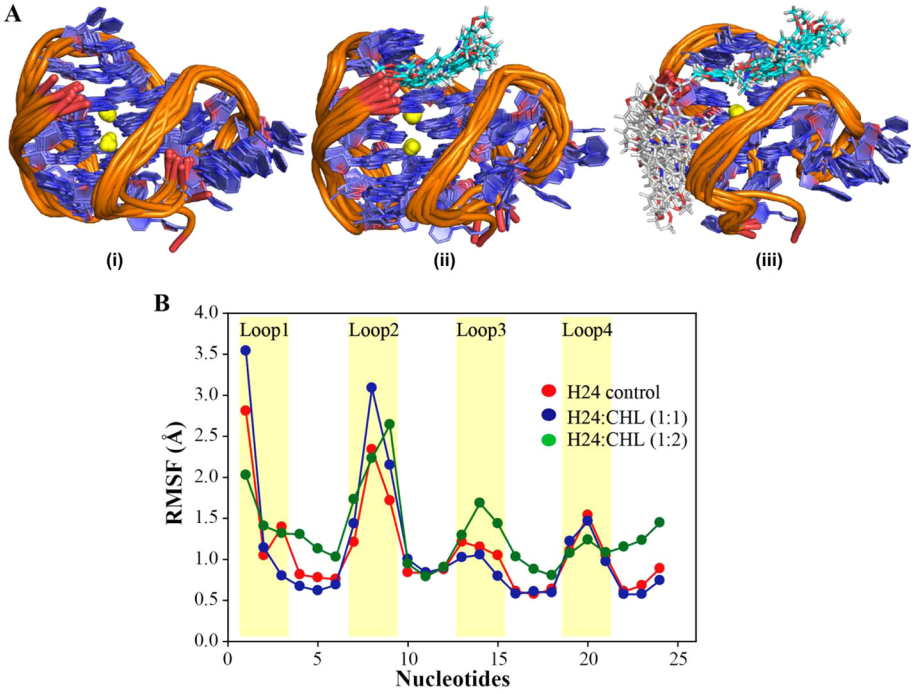

Figure 7. (A) Ensemble of (i) control H24, (ii) H24 and CHL complex in 1:1, and (iii) H24 and CHL complex in 1:2. The ensembles were collected at the interval of 10 ns from MD simulation trajectory. (B) Root mean squared fluctuation (rmsf) of nucleotides from the three models.

H24 under the experimental conditions and concentrations of H24 and CHL.

To further evaluate the context of complexation between H24 and CHL, high resolution NMR spectroscopy was performed. One dimensional proton NMR spectra of H24 alone indicate formation of (3 + 1) type of hybrid structure which is also manifested from the low resolution CD spectroscopy. Addition of CHL to H24 reinforces the faster exchange indicated from their line broadening of N1−H(G) imino proton resonances up to a ratio of 1:1. This phenomenon pointed out oligomerization of H24 in the presence of CHL. The increase in peak intensity at higher CHL concentrations might occur as a sequel to a stable oligomer formation. When the oligomerization starts at a ratio of above 1:1, the transverse relaxation process becomes much faster leading to a faster exchange of the imino protons and hence appearance of sharper imino proton peaks.

DOSY was employed to unearth the process and context of the oligomer/oligomers. We noticed from DOSY that radius of free H24 was almost double as compared to that of complex and there was an approximately six times increase in molecular weight of the complex as compared to the free H24. This might originate due to the formation of a hexamer. We can thus propose a model for the oligomer that is formed due to the interaction of H24 with CHL (Scheme 1): the oligomer contains three planes and each plain contains two H24, each bound to two CHLs. Thus, in the three planes, there are 6 H24s with 12 CHLs to form a unit.

To further elucidate the binding mechanism, MD simulation studies were done. The characteristic features of the association obtained from the thermodynamic calculations based on MD simulation are as follows: (i) CHL association increases the thermodynamic stability of H24, and (ii) binding of the second CHL molecule at the groove perturbs the quartet binding. It is an obvious notion that small molecule binding at the quartet position is physiologically more favorable. This has been inferred from various crystal structures as well as other biophysical and computational studies.[36−38] In the present study, the binding of CHL with G-DNA can be treated as a special case where the protonation of CHL governs the interaction. NMR spectroscopy has confirmed the formation of higher ordered aggregated complexes at and above 1:2 (H24/CHL) ratio. This phenomenon suggests that the interaction is kinetically controlled. CHL has a higher affinity for end-stacking when compared to groove binding. This is evident from the MM-PBSA results (Table 3). The binding energy for 1:1 complex was determined to be −13.6 kcal/mol. The binding free energy for the 1:2 complex formation associated with both mechanisms, (i) and (ii), has been found to be −4.7 and −1.7 kcal/mol, respectively. Hence, it suggests that the propensity of CHL binding to the G-quartet face in the quadruplex is energetically more favorable compared to that of the groove binding. The additive value of binding energy of both CHL with H24 is (−4.7 and −1.7 kcal/mol) −6.4 kcal/mol which is in close agreement with the experimental value obtained from ITC (−7.7 kcal/mol). In the 1:2 complex groove binding, CHL has been found to be more dynamic. This perturbs the backbone conformation which triggers out more dynamicity in the quartet face. This dynamics of the groove bound CHL destabilizes the interaction between the quartet and quartet bound CHL, enforcing less stabilization in the interaction. This event is missing in case of 1:1 complex. The calculation carried out for the 1:2 complex is based on the assumption, that H24 and one CHL act as a receptor for the second CHL molecule which can bind either at the quartet or groove.

We have also analyzed the binding energy values from 70 to 100 ns. These values show that the energies are almost conserved in the last stage of MD simulation (Table S1, Supporting Information). Apart from this, there could be other possible factors to guide the thermodynamic contribution, the

DOI: 10.1021/bi501117x
Biochemistry 2015, 54, 974−986

global overview of which can be best explained by taking consideration of the principal components.

The involvement of coulomb and van der Waal contribution was found to be comparatively less for groove bound CHL as compared to quartet stacked CHL in the 1:2 complex. From the trajectory analysis, it was revealed that the groove bound ligand has more fluctuations and is loosely bound as compared to the quartet stacked CHL. Representation of ensemble structural snapshots (Figure 7A) of the position of groove bound CHL shows its dynamic nature as compared to quartet bound CHL.

Inclusion of the control set within the context of MD simulation along with 1:1 and 1:2 complexes of H24 and CHL provide prospect to differentiate the conformation dynamics in the H24 structure induced by binding of CHL. It is important to have an insight into the conformation of loops, stem and nucleotides to analyze the impact of ligand binding over H24.[39−41] Root mean squared fluctuation (rmsf) of the nucleotides for all the models are represented in Figure 7B. The 5′ terminal end (loop1) nucleotides in all the models of H24 were found to be highly flexible. It is interesting to note that the fluctuations of the residues for H24 control and H24 in 1:1 complex are almost similar. A marked deviation in the fluctuation for loop 3 and 3′ terminal nucleotides in the 1:2 complex is observed when compared to the same of other models. In order to obtain a deeper insight into the respective conformational deviation owing to the presence of ligand, analysis of backbone torsions in the conformational hyperspace was performed. A simplified overview of the ensemble structures can be found in Figure 8 where the groove binding conformation of CHL was found to be markedly dynamic.

The overall structural integrity is well preserved for the conformation of H24 in the course of simulation. The χ angle of the quartets is an important variable in defining G-DNA geometry in (3 + 1) hybrid structure.[42] This angle was found to be well preserved in all the models. Likewise, the sugar puckering angle for the guanine nucleotides, which is another important attribute for nucleic acids, also remains in C2′-*endo* conformation.[43] Deviations were found in the α and γ torsion angles, where variation of the torsion was found to be transient between the gauche (g^+), (g^-) and trans (t) conformation. These variations for the respective nucleotides have been represented qualitatively with the help of various color codes (Figure 8). The difference in the torsion angle values of phosphodiester backbone, ε and ζ, that elucidate BI (negative value) and BII (positive value) are also important. The conformation with respect to BI and BII are found to be similar in both quartet 1 and quartet 3, which seems to remain constant ,whereas only quartet 2 reveals marked difference.

It is noteworthy to mention that computational techniques as such cannot be correlated entirely with experimental means, because there are several factors including the environmental settings, which influence the results. Likewise, there are several constraints included within the computational protocols, which try to impose dummy experimental settings but cannot replace it. A simple assumption is that, in a solution sample, there are various conformations of any complex (bound state) along with the free state of ligand and the receptor. On the contrary, in MD simulation, there is only one representative structure of the complex, believed to denote the most favored conformation of the molecule with the highest population. Similarly, in the present context, there are certain limitations associated with the computational studies, which can affect the real understanding

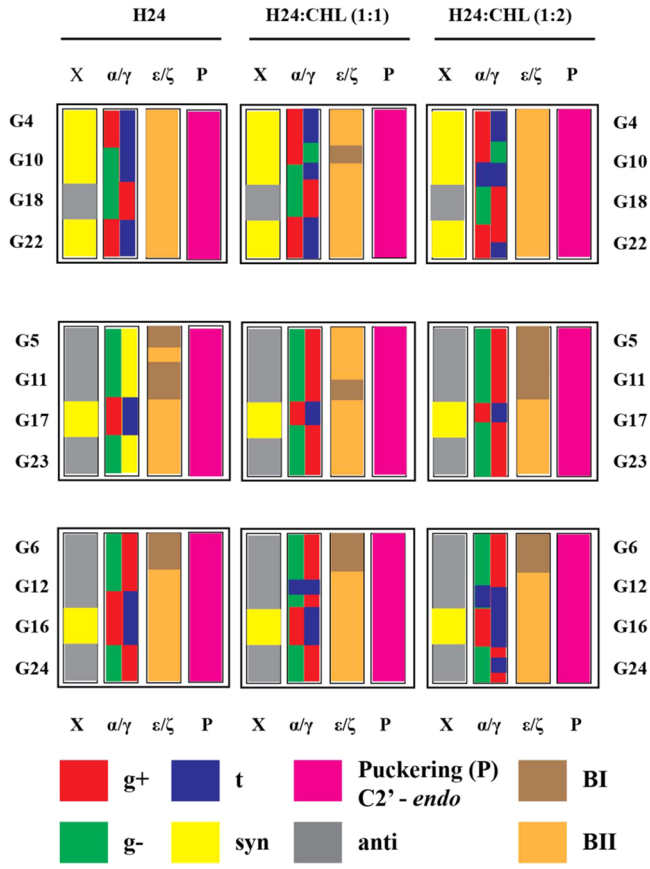

Figure 8. Analysis of conformational variability of H24 from the entire models. Various color codes used for explanation are given in the figure.

of the chemical nature of the interaction.[44,45] The first being that parametrization used for the ligand is based on generalized amber force field. This semiempirical method used for optimization might not fetch the real accurate data. Second, the time scale adopted for the MD simulation is only 100 ns for all models studied. Recent studies from Stadlbauer et al.[46] and Islam et al.[26] provide crucial information that long time simulation is helpful in picking conformational deviation with respect to X-ray structure. Similarly, MD simulation for longer duration can provide more information regarding G-DNA and ligand association. The kinetics of ligand with respect to dissociation and association behavior in the sample solution cannot be included in the atomistic study of molecular modeling. This is another limitation. Hence, it is difficult to figure out the thermodynamics involved in the interaction between H24 and CHL. On the contrary, such explanation can easily be obtained based on experimental studies such as ITC and DSC. Lastly, the aggregation or disaggregation and the equilibrium between different aggregated states of CHL−H24 complex cannot be evaluated by MD simulation.

In spite of these limitations, there are certain crucial information that can be obtained only from molecular modeling. These include (1) visualization of ligand binding with H24, (2) contribution of electrostatics in the association process, (3) information obtained regarding the conformation of the complex in explicit solvent conditions, (4) relative fluctuation of loop nucleotides in the presence and absence of CHL, and (5) torsion angle analysis.

DOI: 10.1021/bi501117x
Biochemistry 2015, 54, 974−986

The data summarizes that the DNA is more stabilized by CHL in 1:2 complex compared to that of the 1:1 complex. The binding phenomena can be proposed to be governed by electrostatic interactions. The difference in binding energy between the two proposed mechanisms suggests that the first CHL molecule binds to the quartet and the second to the groove. The binding of the second molecule in the groove region might assist in the aggregation process of H24.

■ ASSOCIATED CONTENT

Supporting Information

ITC and DSC profile for H24 duplex-chelerythrine interaction, temperature dependent ^{1}H NMR of H24, chelerythrine dependent ^{31}P NMR of H24, RMSD plot, and MMPBSA tables. This material is available free of charge via the Internet at http://pubs.acs.org.

■ AUTHOR INFORMATION

Corresponding Authors

*Telephone: +91-33-2569-3340. Fax: +91-33-2355-3886. E-mail: subhro_c@jcbose.ac.in

*Telephone: +91-33-2337-5345 (extn. 3506). Fax: +91-33-23374637. E-mail: dipak.dasgupta@saha.ac.in.

Author Contributions

§S.G., J.J., and R.K.K. contributed equally

Funding

This work was supported by the intramural grant Biomolecular Assembly, Recognition and Dynamics (BARD) project [Grant Number: 12-R&D-SIN-5.04-0103] from Department of Atomic Energy (DAE), Govt. of India. R.K.K. thanks CSIR for SRF (Grant No. 09/015(0467)/2014-EMR-I). J.J. wants to thank CSIR for funding. S.G. acknowledges funding from Department of Science and Technology (DST) Ramanujan Fellowship [Grant Number: SR/S2/RJN-78/2010 (G)], Govt. of India.

Notes

The authors declare no competing financial interest.

■ ACKNOWLEDGMENTS

The authors thank Chemical Science Division, SINP for the CD experiments.

■ ABBREVIATIONS

5′-TTAGGGTTAGGGTTAGGGTTAGGG-3′-H24, human telomeric DNA sequence; CHL, chelerythrine; TRAP, telomerase repeat amplification protocol; ITC, isothermal titration calorimetry; CDCircular Dichroism, circular dichroism; DSC, differential scanning calorimetry; NMR, nuclear magnetic resonance; MD, molecular dynamics

■ REFERENCES

(1) Hurley, L. H. (2002) DNA and its associated processes as targets for cancer therapy. *Nat. Rev. Cancer 2*, 188−200.

(2) Bearss, D. J., Hurley, L. H., and Von Hoff, D. D. (2000) Telomere maintenance mechanisms as a target for drug development. *Oncogene 19*, 6632−6641.

(3) Neidle, S., and Parkinson, G. (2002) Telomere maintenance as a target for anticancer drug discovery. *Nat. Rev. Drug Discovery 1*, 383−393.

(4) Burge, S., Parkinson, G. N., Hazel, P., Todd, A. K., and Neidle, S. (2006) Quadruplex DNA: Sequence, topology and structure. *Nucleic Acids Res. 34*, 5402−5415.

(5) Ou, T. M., Lu, Y. J., Tan, J. H., Huang, Z. S., Wong, K. Y., and Gu, L. Q. (2008) G-quadruplexes: targets in anticancer drug design. *ChemMedChem 3*, 690−713.

(6) Phan, A. T., Kuryavyi, V., and Patel, D. J. (2006) DNA architecture: from G to Z. *Curr. Opin. Struct. Biol. 16*, 288−298.

(7) Hänsel, R., Loehr, F., Trantirek, L., and Doetsch, V. (2013) High-resolution insights into G-overhang architecture. *J. Am. Chem. Soc. 135*, 2816−2824.

(8) Herbert, J. M., Augereau, J. M., Gleye, J., and Maffrand, J. P. (1990) Chelerythrine is a potent and specific inhibitor of protein kinase C. *Biochem. Biophys. Res. Commun. 172*, 993−999.

(9) Lee, S. K., Qing, W. G., Mar, W., Luyengi, L., Mehta, R. G., Kawanishi, K., Fong, H. H., Beecher, C. W., Kinghorn, A. D., and Pezzuto, J. M. (1998) Angoline and chelerythrine, benzophenanthridine alkaloids that do not inhibit protein kinase C. *J. Biol. Chem. 273*, 19829−19833.

(10) Ghosh, S., Pradhan, S. K., Kar, A., Chowdhury, S., and Dasgupta, D. (2013) Molecular basis of recognition of quadruplexes human telomere and c-myc promoter by the putative anticancer agent sanguinarine. *Biochim. Biophys. Acta 1830*, 4189−4201.

(11) Ghosh, S., Kar, A., Chowdhury, S., and Dasgupta, D. (2013) Ellipticine binds to a human telomere sequence: An additional mode of action as a putative anticancer agent? *Biochemistry 52*, 4127−4137.

(12) Chakrabarti, S., Bhattacharyya, D., and Dasgupta, D. (2001) Structural basis of DNA recognition by anticancer antibiotics, chromomycin A3, and mithramycin: Roles of minor groove width and ligand flexibility. *Biopolymers 56*, 85−95.

(13) Huang, C. Y. (1982) Determination of binding stoichiometry by the continuous variation method: The Job plot. *Methods Enzymol. 87*, 509−525.

(14) Perczel, A., Hollosi, M., Tusnady, G., and Fasman, G. D. (1991) Convex constraint analysis: A natural deconvolution of circular dichroism curves of proteins. *Protein Eng. 4*, 669−679.

(15) Ambrus, A., and Yang, D. (2007) Diffusion-ordered nuclear magnetic resonance spectroscopy for analysis of DNA secondary structural elements. *Anal. Biochem. 367*, 56−67.

(16) Bhunia, A., Domadia, P. N., Mohanram, H., and Bhattacharjya, S. (2009) NMR structural studies of the Ste11 SAM domain in the dodecyl phosphocholine micelle. *Proteins 74*, 328−343.

(17) Phan, A. T., Kuryavyi, V., Luu, K. N., and Patel, D. J. (2007) Structure of two intramolecular G-quadruplexes formed by natural human telomere sequences in K^+ solution. *Nucleic Acids Res. 35*, 6517−6525.

(18) Baker, N. A., Sept, D., Joseph, S., Holst, M. J., and McCammon, J. A. (2001) Electrostatics of nanosystems: Application to microtubules and the ribosome. *Proc. Natl. Acad. Sci. U. S. A. 98*, 10037−10041.

(19) Case, D. A., Cheatham, T. E., 3rd, Darden, T., Gohlke, H., Luo, R., Merz, K. M., Jr., Onufriev, A., Simmerling, C., Wang, B., and Woods, R. J. (2005) The Amber biomolecular simulation programs. *J. Comput. Chem. 26*, 1668−1688.

(20) Perez, A., Marchan, I., Svozil, D., Sponer, J., Cheatham, T. E., 3rd, Laughton, C. A., and Orozco, M. (2007) Refinement of the AMBER force field for nucleic acids: Improving the description of alpha/gamma conformers. *Biophys. J. 92*, 3817−3829.

(21) Wang, J., Wang, W., Kollman, P. A., and Case, D. A. (2006) Automatic atom type and bond type perception in molecular mechanical calculations. *J. Mol. Graphics Modell. 25*, 247−260.

(22) Dang, L. X. (1995) Mechanism and thermodynamics of ion selectivity in aqueous solutions of 18-crown-6 ether: A molecular dynamics study. *J. Am. Chem. Soc. 117*, 6954−6960.

(23) Jorgensen, W. L., Chandrasekhar, J., Madura, J. D., Impey, R. W., and Klein, M. L. (1983) Comparison of simple potential functions for simulating liquid water. *J. Chem. Phys. 79*, 926−935.

(24) Shan, Y., Klepeis, J. L., Eastwood, M. P., Dror, R. O., and Shaw, D. E. (2005) Gaussian split Ewald: A fast Ewald mesh method for molecular simulation. *J. Chem. Phys. 122*, 54101.

(25) Kräutler, V., van Gunsteren, W. F., and Hänenberger, P. H. (2001) A fast SHAKE algorithm to solve distance constraint equations

DOI: 10.1021/bi501117x
Biochemistry 2015, 54, 974−986

for small molecules in molecular dynamics simulations. *J. Comput. Chem. 22*, 501−508.
(26) Islam, B., Sgobba, M., Laughton, C., Orozco, M., Sponer, J., Neidle, S., and Haider, S. (2013) Conformational dynamics of the human propeller telomeric DNA quadruplex on a microsecond time scale. *Nucleic Acids Res. 41*, 2723−2735.
(27) Roe, D. R., and Cheatham, T. E., III. (2013) PTRAJ and CPPTRAJ: software for processing and analysis of molecular dynamics trajectory data. *J. Chem. Theory Comput. 9*, 3084−3095.
(28) Jayaram, B., Sprous, D., and Beveridge, D. (1998) Solvation free energy of biomacromolecules: Parameters for a modified generalized Born model consistent with the AMBER force field. *J. Phys. Chem. B 102*, 9571−9576.
(29) Schlitter, J. R. (1993) Estimation of absolute and relative entropies of macromolecules using the covariance matrix. *Chem. Phys. Lett. 215*, 617−621.
(30) Antonacci, C., Chaires, J. B., and Sheardy, R. D. (2007) Biophysical characterization of the human telomeric (TTAGGG)4 repeat in a potassium solution. *Biochemistry 46*, 4654−4660.
(31) Cui, X., Lin, S., and Yuan, G. (2012) Spectroscopic probing of recognition of the G-quadruplex in c-kit promoter by small-molecule natural products. *Int. J. Biol. Macromol. 50*, 996−1001.
(32) Haq, I. (2002) Thermodynamics of drug-DNA interactions. *Arch. Biochem. Biophys. 403*, 1−15.
(33) Ren, J., Jenkins, T. C., and Chaires, J. B. (2000) Energetics of DNA intercalation reactions. *Biochemistry 39*, 8439−8447.
(34) Pilch, D. S., Barbieri, C. M., Rzuczek, S. G., Lavoie, E. J., and Rice, J. E. (2008) Targeting human telomeric G-quadruplex DNA with oxazole-containing macrocyclic compounds. *Biochimie 90*, 1233−1249.
(35) Ha, J. H., Spolar, R. S., and Record, M. T., Jr. (1989) Role of the hydrophobic effect in stability of site-specific protein-DNA complexes. *J. Mol. Biol. 209*, 801−816.
(36) Dai, J., Carver, M., Hurley, L. H., and Yang, D. (2011) Solution structure of a 2:1 quindoline-c-MYC G-quadruplex: insights into G-quadruplex-interactive small molecule drug design. *J. Am. Chem. Soc. 133*, 17673−17680.
(37) Neil, M., and Keith, I. (2014) Targeting a c-MYC G-quadruplex DNA with a fragment library. *Chem. Commun. 50*, 1704−1707.
(38) Ohnmacht, S. A., Varavipour, E., Nanjunda, R., Pazitna, I., Di Vita, G., Gunaratnam, M., Kumar, A., Ismail, M. A., Boykin, D. W., and Wilson, W. D. (2014) Discovery of new G-quadruplex binding chemotypes. *Chem. Commun. 50*, 960−963.
(39) Stefl, R., Cheatham, T. E., 3rd, Spackova, N., Fadrna, E., Berger, I., Koca, J., and Sponer, J. (2003) Formation pathways of a guanine-quadruplex DNA revealed by molecular dynamics and thermodynamic analysis of the substates. *Biophys. J. 85*, 1787−1804.
(40) Stadlbauer, P., Krepl, M., Cheatham, T. E., 3rd, Koca, J., and Sponer, J. (2013) Structural dynamics of possible late-stage intermediates in folding of quadruplex DNA studied by molecular simulations. *Nucleic Acids Res. 41*, 7128−7143.
(41) Sponer, J., Mladek, A., Spackova, N., Cang, X., Cheatham, T. E., 3rd, and Grimme, S. (2013) Relative stability of different DNA guanine quadruplex stem topologies derived using large-scale quantum-chemical computations. *J. Am. Chem. Soc. 135*, 9785−9796.
(42) Cang, X., Sponer, J., and Cheatham, T. E., 3rd. (2011) Explaining the varied glycosidic conformational, G-tract length and sequence preferences for anti-parallel G-quadruplexes. *Nucleic Acids Res. 39*, 4499−4512.
(43) Sychrovsky, V., Muller, N., Schneider, B., Smrecki, V., Spirko, V., Sponer, J., and Trantirek, L. (2005) Sugar pucker modulates the cross-correlated relaxation rates across the glycosidic bond in DNA. *J. Am. Chem. Soc. 127*, 14663−14667.
(44) Fadrna, E., Spackova, N., Stefl, R., Koca, J., Cheatham, T. E., 3rd, and Sponer, J. (2004) Molecular dynamics simulations of Guanine quadruplex loops: advances and force field limitations. *Biophys. J. 87*, 227−242.
(45) Sponer, J., Cang, X., and Cheatham, T. E., 3rd. (2012) Molecular dynamics simulations of G-DNA and perspectives on the simulation of nucleic acid structures. *Methods 57*, 25−39.
(46) Stadlbauer, P., Trantirek, L., Cheatham, T. E., 3rd, Koca, J., and Sponer, J. (2014) Triplex intermediates in folding of human telomeric quadruplexes probed by microsecond-scale molecular dynamics simulations. *Biochimie 105*, 22−35.

DOI: 10.1021/bi501117x
Biochemistry 2015, 54, 974−986